Dynamical dipole mode in fusion reactions at 16 MeV/nucleon and beam energy dependence

D. Pierroutsakou,[1] B. Martin,[1,2] C. Agodi,[3] R. Alba,[3] V. Baran,[3,4,5] A. Boiano,[1] G. Cardella,[6] M. Colonna,[3] R. Coniglione,[3] E. De Filippo,[6] A. Del Zoppo,[3] M. Di Toro,[3,7] G. Inglima,[1,2] T. Glodariu,[5] M. La Commara,[1,2] C. Maiolino,[3] M. Mazzocco,[8] A. Pagano,[6] C. Parascandolo,[1,2] P. Piattelli,[3] S. Pirrone,[6] C. Rizzo,[3,7] M. Romoli,[1] M. Sandoli,[1,2] D. Santonocito,[3] P. Sapienza,[3] and C. Signorini[8]

[1]*INFN, Sezione di Napoli, via Cintia, 80125 Napoli, Italy*

[2]*Dipartimento di Scienze Fisiche, Università di Napoli "Federico II," via Cintia, 80125 Napoli, Italy*

[3]*INFN, Laboratori Nazionali del Sud, via S. Sofia, 95123 Catania, Italy*

[4]*University of Bucharest, Romania*

[5]*NIPNE-HH, 077125 Magurele, Romania*

[6]*INFN, Sezione di Catania, 95123 Catania, Italy*

[7]*Dipartimento di Fisica, Università di Catania, 95123 Catania, Italy*

[8]*Dipartimento di Fisica and INFN, Sezione di Padova, 35131 Padova, Italy*

(Received 28 April 2009; published 31 August 2009)

High-energy γ rays and light charged particles from the $^{36}\mathrm{Ar} + {}^{96}\mathrm{Zr}$ and $^{40}\mathrm{Ar} + {}^{92}\mathrm{Zr}$ reactions at $E_{\mathrm{lab}} = 16$ and 15.1 MeV/nucleon, respectively, were measured in coincidence with evaporation residues by means of the MEDEA multidetector array coupled to four parallel plate avalanche counters. The aim of this experiment was to investigate the prompt γ radiation, emitted in the decay of the dynamical dipole mode, in the ~16 MeV/nucleon energy range and to map its beam energy dependence, comparing the present results with our previous ones obtained at lower energies. The studied reactions populate, through entrance channels having different charge asymmetries, a compound nucleus in the region of Ce under the same conditions of excitation energy and spin. Light charged particle energy spectra were used to pin down the average excitation energy and the average mass of the system. By studying the γ-ray spectra of the charge symmetric reaction $^{40}\mathrm{Ar} + {}^{92}\mathrm{Zr}$, the statistical giant dipole resonance (GDR) parameters and angular distribution were extracted, and a comparison of the linearized 90° γ-ray spectra of the two reactions revealed a 12% extra yield in the GDR energy region for the more charge asymmetric system. The center-of-mass angular distribution data of this extra γ yield, compatible with a dipole oscillating along the symmetry axis of the dinuclear system, support its dynamical nature. The experimental findings are compared with theoretical predictions performed within a Boltzmann-Nordheim-Vlasov transport model and based on a collective bremsstrahlung analysis of the entrance channel reaction dynamics. An interesting sensitivity to the symmetry term of the equation of state and to in-medium effects on nucleon-nucleon (nn) cross sections is finally discussed.

DOI: 10.1103/PhysRevC.80.024612 PACS number(s): 25.70.Gh, 24.30.Cz

I. INTRODUCTION

The giant dipole resonance (GDR), a collective vibration of protons against neutrons well-established in all the atomic nuclei, can be thermally excited in dissipative heavy-ion reactions as demonstrated by the large body of existing data (for a review, see Refs. [1–3]). Its γ decay, fast enough with respect to other decay modes and with a sizable branching ratio, renders it a powerful probe of the nuclear structure at the emission time under conditions of high temperatures and high spins.

While the thermal GDR features have been widely investigated in the last decades and are well known, the existence of a different GDR-like excitation mode, called pre-equilibrium GDR or dynamical dipole mode, was more recently predicted in various works [4–14]. In charge asymmetric heavy-ion collisions, a large amplitude collective dipole oscillation is expected to occur along the symmetry axis of the deformed composite system because of a nonvanishing dipole moment between the colliding ions. This pre-equilibrium oscillation decays giving rise to a prompt radiation that appears as an extra strength in the energy region of the statistical γ rays coming from the thermal excitation of the GDR in the compound nucleus. It is expected to have a centroid energy lower than that of a GDR in a spherical nucleus of similar mass because of the large deformation of the dinuclear system at the emission moment and a corresponding anisotropic angular distribution pattern. Furthermore, the dependence of its intensity on the beam energy was foreseen in Refs. [10] and [12], with a maximum value in an energy region situated between the low incident energies near the Coulomb barrier and the higher ones near the Fermi energy domain, namely, between 8 and 14 MeV/nucleon.

Experimentally, the existence of the dynamical dipole mode has been studied in deep inelastic [15–17] and fusion heavy-ion collisions [16,18–21] by comparing the γ-ray spectra related with two reactions probing the same composite system under identical conditions of excitation energy and spin but through different charge asymmetry entrance channels. In these measurements, an excess of γ rays was observed in the GDR energy region for the more charge asymmetric partner that was attributed to the decay of the predicted dynamical dipole mode. Although such γ excess constitutes

TABLE I. Reaction pair, incident energy, compound nucleus excitation energy, initial dipole moment $D(t=0)$, initial mass asymmetry Δ, percent increase of the intensity in the 90° linearized γ-ray spectra for the charge asymmetric system (the energy integration was done from 8 to 21 MeV), and centroid energy $E_{\rm dd}$ and width $\Gamma_{\rm dd}$ of the dynamical dipole mode obtained by the fit of the data described in the text.

Reaction	$E_{\rm lab}$ (A MeV)	E^* (MeV)	$D(t=0)$ (fm)	Δ	Increase (%)	$E_{\rm dd}$ (MeV)	$\Gamma_{\rm dd}$ (MeV)
^{32}S + ^{100}Mo	6.125	117	18.2	0.19	1.6 ± 2.0		
^{36}S + ^{96}Mo	5.95	117	1.7	0.16			
^{32}S + ^{100}Mo	9.3	174	18.2	0.19	25 ± 2	11.4 ± 0.3	3.0 ± 0.5
^{36}S + ^{96}Mo	8.9	174	1.7	0.16			
^{36}Ar + ^{96}Zr	16	285 ± 9	20.6	0.16	12 ± 2	12.2 ± 0.6	3.7 ± 1.4
^{40}Ar + ^{92}Zr	15.1	284 ± 9	4.0	0.14			

one of the signatures of the dynamical dipole radiation, angular distribution data are highly desirable to draw a firm conclusion about its origin.

A research project with the aim to map the beam energy dependence of the prompt dipole radiation in fusion reactions was started (described in Refs. [20] and [21]) by studying the same reaction pair at different incident energies and by using the previously described experimental technique. The Ce compound nucleus was formed through the ^{32,36}S + ^{100,96}Mo fusion reactions at excitation energies of 117 MeV ($E_{\rm lab}$ = 6 MeV/nucleon) [21] and 174 MeV ($E_{\rm lab}$ = 9 MeV/nucleon) [20].

In the present work, the prompt dipole emission features are investigated at higher beam energies through the ^{36}Ar + ^{96}Zr and ^{40}Ar + ^{92}Zr fusion reactions at $E_{\rm lab} = 576.9$ and 605.8 MeV ($E_{\rm lab}$ = 16 and 15.1 MeV/nucleon), respectively. The results of this work can be directly compared with those related to the ^{32,36}S + ^{100,96}Mo fusion reactions performed at lower beam energies [20,21] because the above studied reaction pairs form a compound nucleus in the same mass region and they are characterized by the same initial dipole moment difference and a very similar initial mass asymmetry difference. This can be seen in Table I, where we summarize the entrance channel relevant quantities for all the studied reaction pairs leading to compound nuclei in the Ce mass region.

The reaction initial dipole moment $D(t=0)$, shown in the fourth column of Table I, is given by the relation

$$D(t=0) = \frac{NZ}{A}|\overrightarrow{R_Z}(t=0) - \overrightarrow{R_N}(t=0)| = \frac{r_0\left(A_p^{1/3} + A_t^{1/3}\right)}{A} Z_p Z_t \left|\left(\frac{N_p}{Z_p}\right) - \left(\frac{N_t}{Z_t}\right)\right|.$$

Here R_Z and R_N are the center-of-mass coordinates of protons and of neutrons, respectively. $A = A_p + A_t$ is the mass of the composite system and $N = N_p + N_t$ ($Z = Z_p + Z_t$) is its neutron (proton) number; the indices p and t refer to the projectile and target, respectively. The dipole moment changes by 16.6 fm from the ^{40}Ar + ^{92}Zr system to the more N/Z asymmetric one, ^{36}Ar + ^{96}Zr ($r_0 = 1.2$ fm was used to calculate the nuclear radii). The initial mass asymmetry $\Delta = \frac{R_t - R_p}{R_t + R_p}$ of the two reactions differs by a small amount as can be seen in the fifth column of Table I. This small difference does not influence the statistical GDR γ emission, because the studied systems are located above the critical curve in the fissility-mass asymmetry plane [22] where dynamical effects associated with the mass asymmetry are negligible [23]. Furthermore, according to PACE2 [24] calculations, the two reactions have the same critical angular momentum values for fusion and fusion-evaporation (83$\hbar$ and 71$\hbar$, respectively), avoiding thus any difference in the compound nucleus spin distribution.

Pre-equilibrium particle emission occurring at the present beam energies lowers the effective excitation energy and the effective mass of the compound nucleus. To pin down them, the light charged particle energy spectra obtained in coincidence with fusionlike residues were analyzed in the framework of a two moving source scenario. The analysis ensured us that the two considered reactions lead to the formation of a compound nucleus with the same average mass $A = 126$ at the same average excitation energy $E^* = 284$ MeV (shown in the third column of Table I). Therefore, as in our previous works [20,21], all the parameters but the dipole moment were kept identical in the two reactions, so that any difference in their γ-ray spectra can be safely ascribed to the difference in the entrance channel charge asymmetry.

The comparison of these spectra evidenced an extra γ yield for the charge asymmetric reaction with a strongly anisotropic center-of-mass angular distribution that presents a maximum around 90° with respect to the beam axis. The reported anisotropy was much larger than that corresponding to emission of statistical high-energy dipole γ rays from a rotating hot compound nucleus supporting thus the dynamical nature of the associated radiation. Both elements, the observation of a γ-ray excess in the charge asymmetric reaction spectrum and the study of its angular distribution, complete the scenario of the dynamical dipole mode and give important pieces of information about the early stages of fusion dynamics. Moreover, the comparison of the extra γ yield obtained at 16 MeV/nucleon with that obtained at lower beam energies allows one to map its energy dependence. Some of the results reported in this article were published previously in Ref. [25] while preliminary results were presented in Refs. [26–29].

This article is organized as follows: in Sec. II the experimental techniques are discussed. In Sec. III we present the analysis and the obtained results: in Sec. IIIA the energy spectra of the light charged particles are analyzed to evaluate the average excitation energy and average mass of the compound nucleus

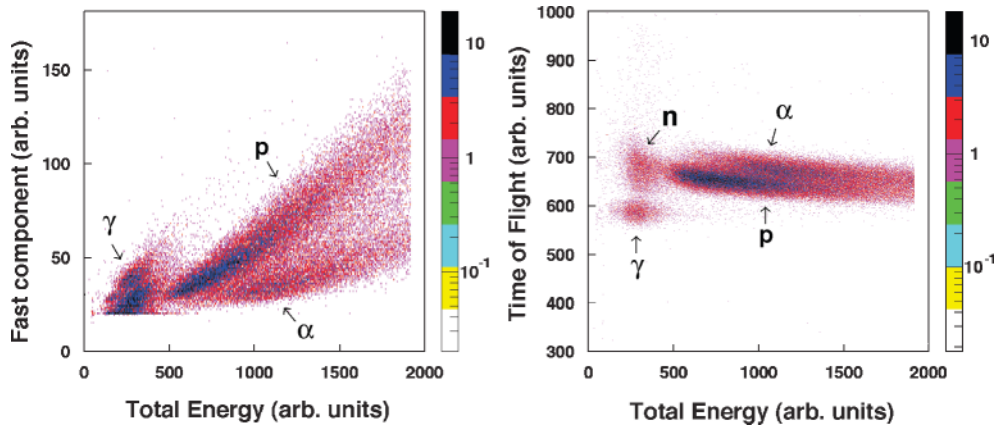

FIG. 1. (Color) Fast component vs Total energy (left-hand side) and Time of flight vs Total energy (right-hand side) bidimensional plots obtained for a BaF_2 in the ring centered at $\theta_{lab} = 51.5^\circ$ in the low gain energy range for the reaction $^{40}Ar + {}^{92}Zr$.

and in Sec. IIIB the γ-ray energy spectra for fusionlike events are shown. The spectrum of the charge symmetric reaction $^{40}Ar + {}^{92}Zr$ is analyzed in the framework of the statistical model while the pre-equilibrium component evidenced in the charge asymmetric reaction spectrum and the associated angular distribution are discussed separately. In Sec. IV the theoretical analysis performed within a Boltzmann-Nordheim-Vlasov (BNV) transport model and based on a collective bremsstrahlung analysis of the reaction dynamics is presented and the results are compared with the experimental findings. Conclusions are drawn in Sec. V.

II. EXPERIMENTAL METHODS

The reactions $^{36}Ar + {}^{96}Zr$ and $^{40}Ar + {}^{92}Zr$ were performed using the ^{36}Ar and ^{40}Ar pulsed beams provided by the Superconducting Cyclotron of the Laboratori Nazionali del Sud (LNS, Italy), impinging on a 450 $\mu g/cm^2$ thick $^{96}ZrO_2$ target (enriched to 95.63% in ^{96}Zr) and on a 600 $\mu g/cm^2$ thick $^{92}ZrO_2$ target (enriched to 95.36% in ^{92}Zr), respectively. The targets were evaporated on carbon layers 90 and 60 $\mu g/cm^2$ thick, respectively. The beam consisted of $\sim$1 ns wide bunches with a 150 ns separation. Beam current was about 2 nA.

The γ rays and the light charged particles were detected by using the 180 barium fluoride (BaF_2) modules of the MEDEA experimental apparatus (for more details, see Ref. [30]) that covers the polar angular range between $\theta_{lab} = 30^\circ$ and $\theta_{lab} = 170^\circ$ and the full range in the azimuthal angle ϕ. The crystals are arranged in eight rings, each of them located at a fixed angle. The MEDEA ball has an inner radius of 22 cm and covers a total solid angle of 3.7π sr. The apparatus operates under vacuum inside a large scattering chamber to allow a simultaneous detection of γ rays and light charged particles. Only seven among the eight rings were used in the present experiment, positioned at $\theta_{lab} = 51.5^\circ$, 68.1°, 82.8°, 97.1°, 111.9°, 128.5°, and 159.7°.

The discrimination between γ rays and light charged particles was performed by combining a pulse shape analysis of the BaF_2 signal with a time of flight measurement, achieved with a resolution of $\sim$1 ns, between each BaF_2 detector and the radiofrequency signal of the cyclotron.

The PM output of each BaF_2 module was split into four, differently weighted, signals. One was used for timing, two were used for energy integration in two different dynamical ranges (about 30 and about 200 MeV full scale, respectively), and one was used to integrate the BaF_2 fast light emission component. The combination of this last information with the energy information allows us to obtain a shape analysis of the BaF_2 response so as to identify photons and light charged particles.

In Fig. 1, "Fast component vs Total energy" (left-hand side) and "Time of flight vs Total energy" (right-hand side) bidimensional plots are shown, obtained during the reaction $^{40}Ar + {}^{92}Zr$ for a detector in the ring centered at $\theta_{lab} = 51.5^\circ$ in the low gain energy range.

By applying contours to both these planes, an unambiguous discrimination between γ rays, protons, and α particles is achieved. Low-energy neutrons ($E_n \leqslant 20$ MeV), giving the same pulse shape as γ rays, are separated by the time of flight measurements [31]; high-energy neutrons ($E_n >$ 20 MeV), giving a pulse shape similar to the proton one, are separated from the γ rays in the "Fast component vs Total energy" plot [32]. The same procedure was applied for the high gain energy range. The energy calibration of the γ-ray detectors was obtained by using the composite sources of $^{241}Am + {}^{9}Be$ and $^{238}Pu + {}^{13}C$ and the 15.1 MeV γ rays from the $p + {}^{12}C$ reaction. The charged particle calibration was deduced from the γ calibration as described elsewhere [33]. The time stability of the energy calibration was checked during the experiment by monitoring after each run the stability of the peak corresponding to a radioactive source.

The fusion-evaporation residues were detected by four position-sensitive parallel plate avalanche counters (PPACs) located symmetrically around the beam direction at 70 cm from the target. The PPACs were centered at an angle of $\theta_{lab} = 7^\circ$ with respect to the beam direction, subtending 7° in θ. The total solid angle covered by the PPACs was 0.089 sr. They provided the time of flight (TOF) signal with respect to the radiofrequency signal of the cyclotron and the energy loss (ΔE) of the reaction products. In Fig. 2 the "Energy loss vs Time of flight" bidimensional plot, obtained for one of the PPACs during the reaction $^{40}Ar + {}^{92}Zr$, is shown.

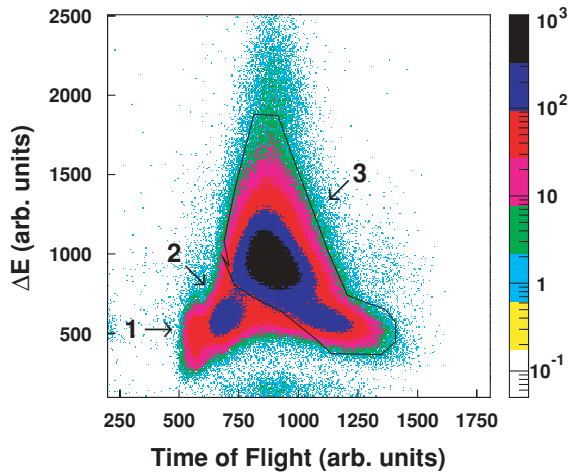

FIG. 2. (Color) Energy loss vs Time of Flight bidimensional plot obtained for one of the PPACs during the reaction $^{40}\mathrm{Ar} + {}^{92}\mathrm{Zr}$ (singles and coincidence events). The events located inside the contour are retained for the analysis.

A relative TOF calibration was achieved by considering the distance between the elastic peaks observed during two runs characterized by fixed delays in the radiofrequency signal. The locus at small TOF and low ΔE (marked with a 1 in the figure) indicates events where the projectile was elastically scattered by the target. The locus characterized by low ΔE but longer TOF (marked with a 2) corresponds to peripheral and/or fission events. The region showing a maximum at large ΔE (marked with a 3) corresponds to the detection of the fusionlike residues. The tail extending toward longer TOF is due to incomplete momentum transfer events. In the analysis the fusionlike events included in the contour shown in Fig. 2 were retained. For both reactions, the mean residue velocity of the considered events was found to be equal to 90% of the center-of-mass velocity for complete fusion. Down-scaled single events together with coincidence events between a PPAC and at least one fired BaF_2 scintillator were collected during the experiment. A coincidence event was accepted if the deposited energy in a BaF_2 detector was greater than ∼5.5 MeV for γ rays. The coincidence request eliminated any cosmic ray contamination of the γ-ray spectra.

III. ANALYSIS AND RESULTS

Incomplete fusion is expected to be important at the present beam energies [34]. This kind of event cannot be discarded in the time of flight spectrum of the reaction products because they have velocity distributions overlapping with those of the complete fusion reactions [35,37].

Incomplete fusion events are characterized by emission of pre-equilibrium light particles that reduces the compound nucleus average mass, average charge, and average excitation energy. In the present work, the average excitation energy and the average mass of the composite system after pre-equilibrium particle emission were evaluated by studying the energy spectra of the charged particles detected in coincidence with evaporation residues while the pre-equilibrium neutron emission was estimated from our proton data and from existing neutron emission studies (Ref. [36] and references therein).

A. Charged particle spectra

The proton and α-particle kinetic energy spectra in the laboratory reference frame in coincidence with the fusionlike residues of the contour in Fig. 2, obtained at several angles covering between $51^\circ < \theta_{\mathrm{lab}} < 160^\circ$, are reported in Figs. 3 and 4 for the $^{40}\mathrm{Ar} + {}^{92}\mathrm{Zr}$ (left-hand side) and $^{36}\mathrm{Ar} + {}^{96}\mathrm{Zr}$ (right-hand side) reactions, respectively.

These spectra were analyzed by means of a moving source fit in which the particles were assumed to be emitted isotropically from two moving sources: a *slow* source describing the statistical evaporation from the hot compound nucleus and an *intermediate-velocity* (between the compound nucleus and the projectile velocity) source related to the pre-equilibrium particles emitted by the composite system before thermalization.

The energy distribution of the evaporated particles was parametrized, in the source rest frame, adopting a surface-type Maxwellian distribution given by

$$\left(\frac{d^2M}{d\Omega dE}\right)_{\mathrm{sl}} = \frac{M_{\mathrm{sl}}}{4\pi T_{\mathrm{sl}}^2}\,(E - E_c)\,\exp\left[-\frac{(E - E_c)}{T_{\mathrm{sl}}}\right], \quad (1)$$

while the distribution of the pre-equilibrium particles was taken to be that for volume emission from a thermal source,

$$\left(\frac{d^2M}{d\Omega dE}\right)_{\mathrm{int}} = \frac{M_{\mathrm{int}}}{2(\pi T_{\mathrm{int}})^{3/2}}\sqrt{E - E_c}\,\exp\left[-\frac{(E - E_c)}{T_{\mathrm{int}}}\right], \quad (2)$$

where E is the particle energy, E_c is the Coulomb barrier for particle emission, T_i (i is for "sl" or "int") is the apparent source temperature, and M_i is the multiplicity of the particles emitted from the i source. Both Maxwellian distributions were transformed in the laboratory reference frame using the relation

$$\left(\frac{d^2M}{d\Omega dE}\right)_{\mathrm{lab}} = \sqrt{\frac{E_{\mathrm{lab}}}{E'}}\left(\frac{d^2M}{d\Omega dE}\right)_{E=E'}, \quad (3)$$

where the particle energy E' in the source reference frame is given by

$$E' = E_{\mathrm{lab}} + E_s - 2\sqrt{E_{\mathrm{lab}}\,E_s}\,\cos\theta_{\mathrm{lab}}, \quad (4)$$

where E_s is the energy of a particle moving with the source velocity, assumed to be parallel to the beam axis and θ_{lab} is the observation angle of the particle.

The evaporative source velocity was fixed to a value equal to 90% of the center-of-mass velocity, namely, $v_{\mathrm{sl}} = 1.46$ cm/ns and 1.36 cm/ns for the systems $^{40}\mathrm{Ar} + {}^{92}\mathrm{Zr}$ and $^{36}\mathrm{Ar} + {}^{96}\mathrm{Zr}$, respectively, as determined by the calibration of the PPACs TOF spectra. The remaining five parameters were considered as free variables in the fitting procedure. It was found that the data could be fitted with the same value of the Coulomb barrier E_c for both sources. It was fixed $E_c = 4$ MeV for protons and $E_c = 10$ MeV for α particles. It should be noted that the

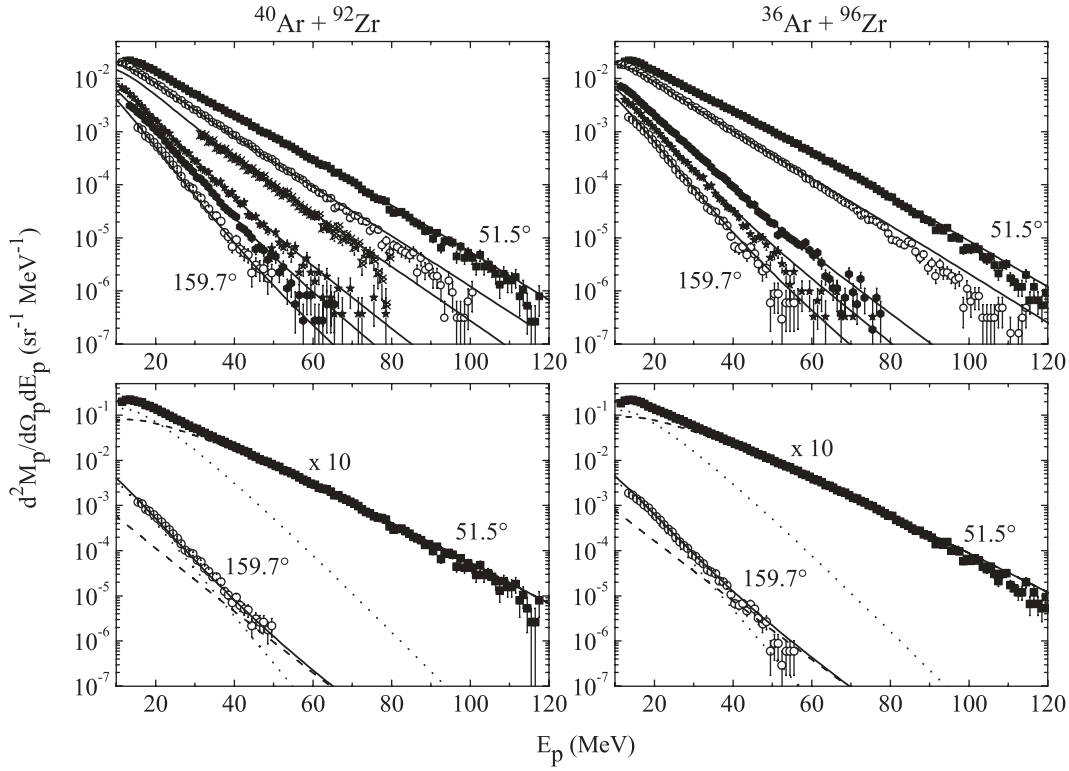

FIG. 3. (Top) Laboratory proton energy spectra obtained at various angles in coincidence with the fusionlike residues. For the ^{40}Ar + ^{92}Zr reaction the angles are 51.5°, 68.1°, 82.8°, 111.9°, 128.5°, and 159.7°. For the ^{36}Ar + ^{96}Zr reaction the angles are 51.5°, 68.1°, 111.9°, 128.5°, and 159.7°. The solid lines show the results of the simultaneous fits described in the text. (Bottom) Laboratory proton energy spectra at two angles. The solid lines are the results of the fits with two sources. The dashed and dotted lines represent the intermediate-velocity source and the slow source components, respectively.

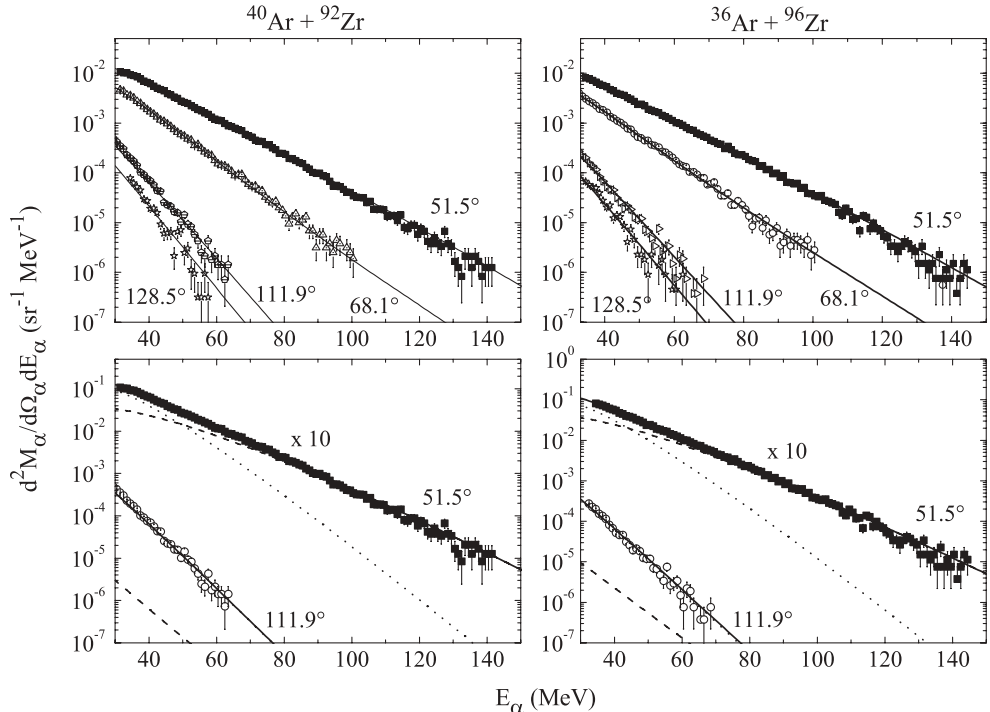

FIG. 4. (Top) Laboratory α-particle energy spectra obtained at various angles in coincidence with the fusionlike residues. The solid lines are the results of the simultaneous fits described in the text. (Bottom) Laboratory α-particle energy spectra at two angles. The solid lines are the results of the fits with two sources. The dashed and dotted lines represent the intermediate-velocity source and the slow source components, respectively.

TABLE II. Multiplicities, temperatures, and velocities of the slow and the intermediate-velocity sources extracted from the moving source fit for protons emitted during the $^{40}Ar + ^{92}Zr$ and $^{36}Ar + ^{96}Zr$ fusion reactions.

Reaction	E_c (MeV)	v_{sl} (cm/ns)	M_{sl}	T_{sl} (MeV)	v_{int} (cm/ns)	M_{int}	T_{int} (MeV)
$^{40}Ar + ^{92}Zr$	4	1.46	1.74 ± 0.06	4.36 ± 0.08	3.30 ± 0.12	1.28 ± 0.04	7.89 ± 0.13
$^{36}Ar + ^{96}Zr$	4	1.36	1.66 ± 0.04	4.44 ± 0.06	3.27 ± 0.07	1.54 ± 0.02	8.23 ± 0.08

sensitivity of the fit to reasonable changes of the Coulomb barrier values is small.

The results of the simultaneous fits are shown with solid lines in the top of Figs. 3 and 4 for protons and α particles, respectively. The relative contributions of the two sources are reported in the bottom of the same figures for a backward and a forward angle, with the slow (intermediate-velocity) source component represented with a dotted (dashed) line. The parameters extracted from the fit (multiplicity, and temperature of the slow source and multiplicity, temperature and velocity of the intermediate-velocity source) are reported in Tables II and III for protons and α particles, respectively. The quoted uncertainties correspond to the change in a parameter that increases χ^2 by 1, with all the other parameters fixed at their optimum values.

To evaluate the average energy taken away by pre-equilibrium neutrons, not detected in the present experiment, we assumed that their energy spectra were very similar to the proton ones, apart from the Coulomb barrier. Then, the average kinetic energy of a pre-equilibrium neutron was taken to be that of a pre-equilibrium proton minus the Coulomb barrier while the pre-equilibrium neutron multiplicity was deduced by that of pre-equilibrium protons multiplied with the N/Z ratio of the projectile. The adopted pre-equilibrium neutron multiplicity, 1.54 ± 0.25 for both reactions, is in agreement within errors with neutron emission studies performed at similar center-of-mass incident energy above the Coulomb barrier [36]. The values of average kinetic energy, binding energy, and energy lost for each pre-equilibrium particle can be seen for the $^{40}Ar + ^{92}Zr$ and $^{36}Ar + ^{96}Zr$ reactions in Tables IV and V, respectively. The average excitation energy of the composite system after pre-equilibrium particle emission, $E^* = E_{CM} + Q_{gg} - E_{lost}$, with E_{CM} being the energy available in the center-of-mass reference frame, Q_{gg} the reaction Q value, and E_{lost} the total energy lost, was deduced to be $E^* = (284 \pm 9)$ MeV for the $^{40}Ar + ^{92}Zr$ reaction and $E^* = (285 \pm 9)$ MeV for the $^{36}Ar + ^{96}Zr$ reaction, while its average mass was found to be $A = 126$ for both reactions. Therefore, because the average excitation energy and the average mass of the composite system after pre-equilibrium particle emission are the same within errors for the two reactions, we can proceed in the comparison of their γ-ray spectra, being confident that any difference between them is an entrance channel effect.

B. γ spectra

In Fig. 5 we show the center-of-mass γ-ray spectra in coincidence with fusionlike residues. The spectra of the BaF_2 rings placed at 82.8° and 97.1° were summed and the resulting spectrum is referred to as the 90° spectrum.

Before a comparison of the γ-ray spectra between the two reactions in the GDR energy region can be performed, the incoherent bremsstrahlung component, considered to originate primarily in neutron-proton (np) collisions and dominant for $E_\gamma > 35$ MeV, must be evaluated and subtracted. An equal bremsstrahlung component is expected for the $^{36,40}A + ^{96,92}Zr$ reactions because of their very similar beam energy and size of the reaction partners and of the same temperature of the composite system (see Ref. [38] and references therein). This is largely confirmed by the data of the two reactions, which are equal within errors for $E_\gamma \geqslant 21$ MeV and for all the considered angles.

Because the bremsstrahlung contribution is equal in both reactions, its subtraction from the data is necessary for the study of the spectrum and angular distribution of the γ rays emitted in each reaction, presented in the following, but it does not affect the spectrum and the angular distribution referring to the difference between the data of the two reactions.

The np bremsstrahlung component was deduced by fitting simultaneously the center-of-mass high-energy ($E_\gamma \geqslant 35$ MeV) γ-ray spectra of both reactions at different angles assuming an exponentially decreasing behavior in the nn center-of mass system of the type

$$\left(\frac{d^2M}{d\Omega dE_\gamma}\right) = N_\gamma * \exp\left(-\frac{E_\gamma}{E_0}\right) \tag{5}$$

and an emitting source moving with 0.5 v_{beam} [39]. The inverse slope of the spectra was found to be $E_0 = (8.8 \pm 1.3)$ MeV, in good agreement with the systematics for bremsstrahlung spectra. The results of the simultaneous fits are shown with the solid lines in Fig. 5.

TABLE III. Same as in Table II but for α particles.

Reaction	E_c (MeV)	v_{sl} (cm/ns)	M_{sl}	T_{sl} (MeV)	v_{int} (cm/ns)	M_{int}	T_{int} (MeV)
$^{40}Ar + ^{92}Zr$	10	1.46	1.77 ± 0.08	5.63 ± 0.11	3.60 ± 0.17	0.90 ± 0.06	7.78 ± 0.22
$^{36}Ar + ^{96}Zr$	10	1.36	1.47 ± 0.10	5.61 ± 0.11	3.21 ± 0.17	0.81 ± 0.05	8.13 ± 0.22

TABLE IV. Average kinetic energy E_k, binding energy $E_{\rm bind}$, pre-equilibrium particle multiplicity $M_{\rm int}$, and average energy lost $E_{\rm lost}$ for the ^{40}Ar + ^{92}Zr reaction.

Particle	E_k (MeV)	$E_{\rm bind}$ (MeV)	$M_{\rm int}$	$E_{\rm lost} = M_{\rm int}*[E_k + E_{\rm bind}]$ (MeV)
Proton	17.6 ± 0.3	5.96	1.28 ± 0.04	30.1 ± 1.0
Neutron	13.6 ± 0.3	10.9	1.54 ± 0.25	37.7 ± 6.1
α	31.2 ± 1.5	-0.5	0.90 ± 0.06	27.6 ± 2.3

The lack of statistics for γ rays with $E_\gamma > 30$ MeV prevented us from performing a fit with two exponential functions that should simulate adequately the thermal and the direct components of np bremsstrahlung emission (see Refs. [40] and [38] and references therein). Our procedure ensures that at least the direct (first chance) bremsstrahlung component was properly subtracted from our spectra. However, being that the compound system is identical in mass and has the same temperature for the two considered reactions, the thermal bremsstrahlung component is expected to be the same (see, for instance, Ref. [38]) and this is confirmed by our data, as mentioned previously. Therefore, an eventual residual contamination due to an incomplete subtraction of this component, expected to be emitted isotropically in the center-of-mass frame [41], will disappear in the difference without affecting our results concerning the pre-equilibrium dipole emission.

1. GDR in the charge symmetric reaction

In the case of the charge symmetric reaction, the γ-ray spectrum after bremsstrahlung subtraction can be adequately reproduced using the statistical decay code CASCADE [42].

In the left-hand side of Fig. 6 we report the 90° bremsstrahlung-subtracted γ-ray spectrum of the ^{40}Ar + ^{92}Zr reaction (circles) together with theoretical spectra obtained with the code CASCADE for the same reaction and folded with the response function of the experimental apparatus [43]. The error bars in the data include both the statistical uncertainties and the errors due to the subtraction of the bremsstrahlung radiation. The data can be reproduced well in the whole energy region of interest by using the following parameters in the calculation (solid line in the figure): a compound nucleus mass $A = 126$, $E^* = 284$ MeV, as obtained by the charged particle spectra analysis, and a level density parameter varying with nuclear temperature as described in Ref. [44] and in Ref. [26] therein. The GDR strength function was taken to be a lorentzian curve with centroid energy $E_{\rm GDR} = 14$ MeV, width $\Gamma_{\rm GDR} = 13$ MeV, and strength $S_{\rm GDR} = 100\%$ of the $E1$ energy-weighted sum-rule strength throughout the calculation. Moreover, a cutoff in the γ-ray emission for excitation energies larger than $E^* \sim 250$ MeV must be applied in the calculation to reproduce the data, in good agreement with Ref. [45] for nuclei in the $A \sim 115$ mass region. To evidence that in absence of this cutoff the theoretical spectra overestimate the γ yield, we present in the same figure, with the dashed line, the CASCADE calculation where the same parameters as previously were used but without cutoff in the γ emission. We observe that the theoretical γ yield becomes larger than the experimental one for $E_\gamma > 10$ MeV. The sensitivity of the theoretical spectra to the compound nucleus excitation energy can be seen if we compare the dashed and the dotted lines of the figure. The dotted line corresponds to a CASCADE calculation identical to that of the dashed one but with $E^* = 274$ MeV. In the right-hand side of Fig. 6, we show the influence of the GDR strength in the calculation. The theoretical spectra were obtained by using in the CASCADE code $E^* = 284$ MeV and the same parameters as previously, without any cutoff in the γ emission and by changing the GDR strength from 100% (solid line) to 92% (dashed line) and to 80% (dotted line) of the $E1$ energy-weighted sum-rule strength throughout the calculation. We see that there is no way to reproduce the data by changing the GDR strength if γ emission is allowed to occur for excitation energies as high as $E^* = 284$ MeV. Moreover, the use of a constant level density parameter instead of one varying with nuclear temperature even worsens the quality of the fit.

Therefore in the present work, we confirm a suppression of the GDR γ emission for energies above $E^* \sim 2$ MeV/nucleon for $A = 126$, in reasonable agreement with the value of $\sim$2.5 MeV/nucleon extracted previously for nuclei with similar mass ([45–47]. The same suppression was observed also for lighter nuclei, $A = 60$–70, at higher excitation energies ($E^* \sim 5$ MeV/nucleon) [16], denoting a mass dependence of the limiting excitation energy for the collective motion that is very similar to the mass dependence of the limiting temperature that nuclei can sustain [48]. The above observations show that there is a limit up to which nuclei exhibit collective behavior, then a transition from order to chaos sets in. The interesting hypothesis of a link between such an order to chaos transition

TABLE V. Same as in Table IV but for the ^{36}Ar + ^{96}Zr reaction.

Particle	E_k (MeV)	$E_{\rm bind}$ (MeV)	$M_{\rm int}$	$E_{\rm lost} = M_{\rm int}*[E_k + E_{\rm bind}]$ (MeV)
Proton	18.2 ± 0.2	5.96	1.54 ± 0.02	37.3 ± 0.6
Neutron	14.2 ± 0.2	10.9	1.54 ± 0.25	39.0 ± 6.3
α	29.3 ± 1.3	-0.5	0.81 ± 0.05	23.3 ± 1.8

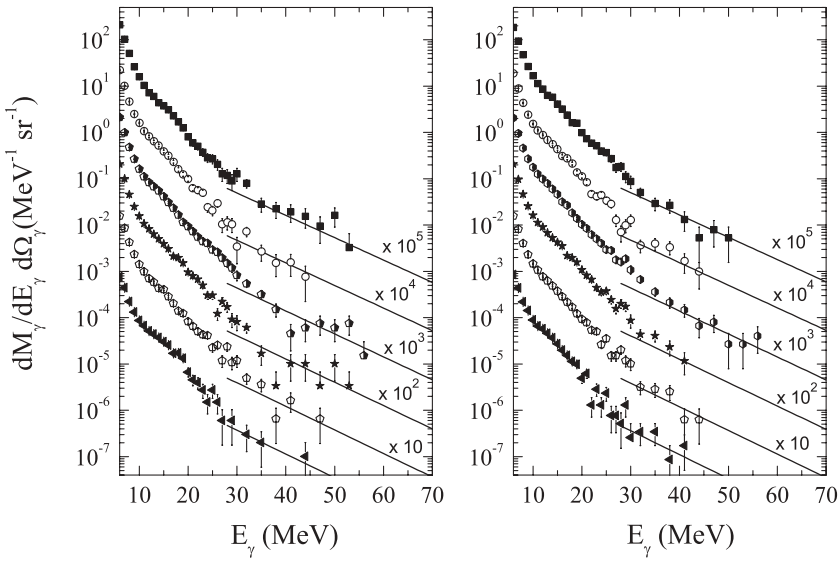

FIG. 5. Center-of-mass γ-ray spectra in coincidence with the fusionlike residues for different laboratory angles (from top to bottom: θ = 51.5°, 68.1°, 90°, 111.9°, 128.5°, 159.7°) for the ^{40}Ar + ^{92}Zr (left-hand side) reaction and the ^{36}Ar + ^{96}Zr (right-hand side) reaction. The solid lines represent the bremsstrahlung components determined from the simultaneous fits of the data, as described in the text and they are displayed down to 28 MeV for clarity reasons.

and a liquid-gas phase transition, claimed to occur at similar nuclear excitation energies, deserves further investigation [for a review, see Ref. [3]).

2. *Pre-equilibrium component*

In Fig. 7 the γ spectra of the two reactions obtained at $\theta_{\rm lab}$ = 90° resulting after the subtraction of the *np* bremsstrahlung component are presented. The stars in the same figure represent the difference between the data of the two reactions. From this figure, one can see that the γ-ray multiplicity related with the charge asymmetric reaction is clearly larger than that of the charge symmetric one. This excess cannot be ascribed to differences in the statistical GDR in the compound nucleus formed in the two reactions, being identical all the reaction parameters, except for the entrance channel charge asymmetry. Therefore, it is related to entrance channel charge asymmetry effects and it is attributed to the dynamical dipole mode present at the beginning of the dinuclear system formation.

To better evidence details in the GDR energy region for the present work, the data (solid squares and open circles of Fig. 7) and the charge symmetric reaction theoretical γ-ray spectrum (solid line of the left-hand side of Fig. 6) are linearized, dividing them by the same theoretical spectrum. The latter was obtained by using the code CASCADE with the same parameters as described previously (see parameters for the solid line of Fig. 6, left-hand side) but with a constant dipole strength function instead of a lorentzian one and folded by the response function of the experimental apparatus. The resulting linearized data and linearized theoretical spectrum are shown in Fig. 8. By integrating over energy these data, from 8 to 21 MeV, a 12% increase of the γ-ray intensity is found in the charge asymmetric system. From Table I, where the percent increase of the 90° linearized spectra for the studied three beam energies is shown, we can see that the prompt dipole radiation intensity presents a maximum at 9 MeV/nucleon decreasing toward lower and higher energies. Although diminished with respect to its value at 9 MeV/nucleon, it is still observed at

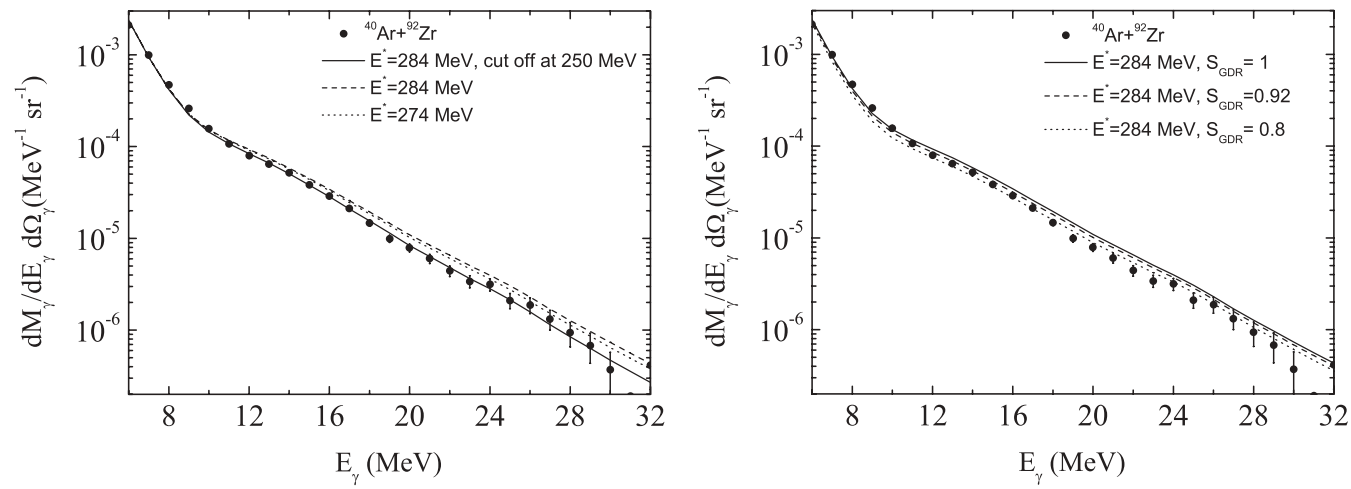

FIG. 6. 90° bremsstrahlung-subtracted γ-ray spectra of the charge symmetric reaction ^{40}Ar + ^{92}Zr (circles) and theoretical spectra (lines) calculated with the code CASCADE for the same reaction as described in the text.

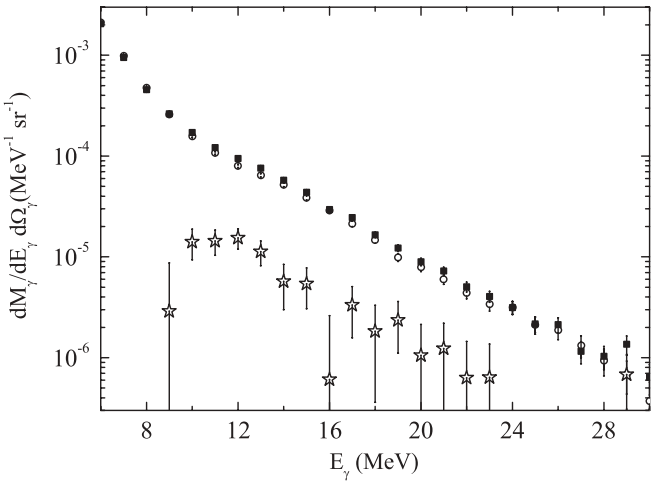

FIG. 7. 90° bremsstrahlung-subtracted γ-ray spectra in coincidence with the fusionlike residues for the ^{40}Ar + ^{92}Zr (open circles) and for the ^{36}Ar + ^{96}Zr (solid squares) reaction. The stars represent the difference between the two spectra.

nuclear excitation energies as high as ∼280 MeV, excluding a fast increase of the dynamical dipole mode damping width with excitation energy. In fact the dynamical dipole mode is a pre-equilibrium collective oscillation present before the thermalization of the mechanical energy. The damping is then also related to fast processes, the pre-equilibrium nucleon emissions (mostly neutrons, that are reducing the charge asymmetry), and (p,n) direct collisions that will damp the isovector oscillation. From calculations we expect that both mechanisms are smoothly increasing in the present range of beam energies.

In this subsection we analyze the pre-equilibrium component observed at two beam energies, namely, at 9 and 16 MeV/nucleon, to deduce the characteristics of the dynamical dipole mode and their evolution with beam energy.

In Fig. 9 we report the difference spectra obtained for the ^{32,36}S + ^{100,96}Mo reactions at 9 MeV/nucleon (left-hand side) and for the ^{36,40}Ar + ^{96,92}Zr reactions at 16 MeV/nucleon (right-hand side). The centroid energy E_{dd} and the width Γ_{dd} of the dynamical dipole mode were extracted fitting the observed γ-ray excess with a lorentzian curve folded by the corresponding experimental apparatus response function (solid lines in the figure). The values obtained from the fit are reported in Table I. It is worth noting that for both beam energies, E_{dd} was found to be lower than the centroid energy of the compound GDR ($E_{GDR} = 14$ MeV), implying a deformation of the composite system at the moment of the prompt dipole radiation. In a naive picture of two colliding nuclei at the touching configuration, we expect $E_{dd} \sim \frac{78}{A_1^{1/3}+A_2^{1/3}} \sim 10$ MeV, A_1 and A_2 being the colliding ion masses. The fact that it was found to be somewhat larger than predicted is consistent with the expectation that some density overlap already exists at the start-up of the dipole oscillation [10]. We notice that centroid energy and width remain constant within errors by increasing the beam energy.

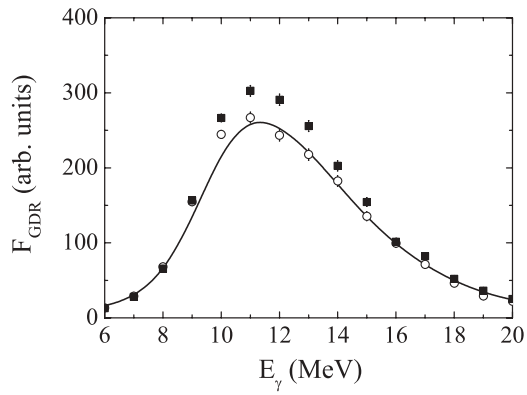

FIG. 8. 90° bremsstrahlung-subtracted γ-ray spectra of the ^{40}Ar + ^{92}Zr (open circles) reaction and the ^{36}Ar + ^{96}Zr (solid squares) reaction, linearized as described in the text. The solid line represents the theoretical spectrum calculated with the code CASCADE for the charge symmetric reaction ^{40}Ar + ^{92}Zr linearized as described in the text.

3. *Angular distributions*

To obtain a clear signature about the nature of the extra γ yield seen in the charge asymmetric reaction, we display in Figs. 10, 11, and 12 the center-of-mass angular distribution with respect to the beam direction of the observed γ rays for the ^{36,40}Ar + ^{96,92}Zr reactions integrated over energy in the following intervals: from 10 to 14, 15 to 17, and 18 to 20 MeV, respectively. The angular distributions are corrected by the experimental setup efficiency obtained from the response function of the apparatus [43]. We remind the reader that no normalization of the γ-ray spectra was done, because we measured the double differential γ-ray multiplicity for fusion-evaporation events. In the top portions of the above figures we report the data for the two reactions, charge asymmetric (solid squares) and symmetric (open circles), while in the bottom portions we show the angular distribution of the difference between the data displayed in the top portion of the respective figure. We notice that the charge asymmetric reaction diplays a more anisotropic angular distribution around 90°. Because we have selected the same compound nucleus, with the same excitation energy and angular momentum, such a difference in the γ-ray angular distributions should be ascribed to entrance channel effects.

The lines in the top panels of the above figures depict the expected angular distribution of the γ rays emitted in the charge symmetric reaction given by the Legendre polynomial expansion $M_\gamma(\theta_\gamma) = M_0[1 + Q_2 a_2 P_2(\cos(\theta_\gamma)]$, where a_2 is the anisotropy coefficient and Q_2 is an attenuation factor for the finite γ-ray counter, which, for the present geometry, was found to be ∼0.98 [49]. In all cases, the coefficient M_0 was obtained from a best fit to the data. It was verified for all the angular distributions presented here that odd order coefficients in the Legendre polynomial expansion are zero within errors. The a_2 anisotropy coefficients that fit the symmetric reaction data are -0.22 ± 0.04 for $10\,\text{MeV} \leqslant E_\gamma \leqslant 14\,\text{MeV}$, -0.14 ± 0.06 for $15\,\text{MeV} \leqslant E_\gamma \leqslant 17\,\text{MeV}$, and -0.03 ± 0.10 for $18\,\text{MeV} \leqslant E_\gamma \leqslant 20\,\text{MeV}$. Because the γ rays in the symmetric reaction come from the statistical GDR decay, where all

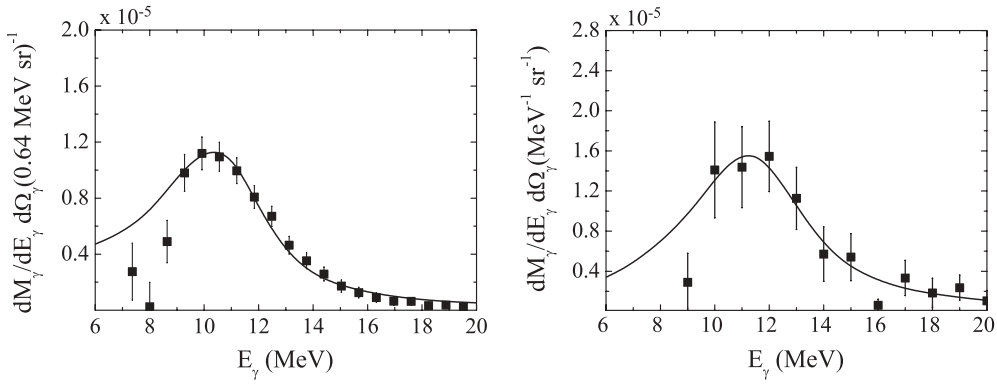

FIG. 9. 90° difference spectra of the ^{32,36}S + ^{100,96}Mo reactions at 9 MeV/nucleon (left-hand side) and of the ^{36,40}Ar + ^{96,92}Zr reactions at ∼16 MeV/nucleon (right-hand side). The solid line is a fit of the data as described in the text.

rotating angles are probed by the compound nucleus (see the discussion later in the same paragraph), the a_2 coefficient is expected to have an energy dependence characteristic of statistical GDR γ decay in a hot rotating nucleus of average mass $A = 126$ and of mean spin $I = 47$–$50\hbar$. The energy dependence of the center-of-mass angular distribution coefficient a_2 for the symmetric reaction data can be seen in more detail in Fig. 13 for a 1 MeV energy bin. In a rotating, not collectively oblate compound nucleus, as in the present case, the two low-energy GDR components (along the two longer axes) should have a minimum $a_2 \sim -0.25$ (stretched dipole transitions) while the upper-energy GDR component should have an $a_2 \sim 0.5$ (unstretched dipole transition) [1] with some attenuation because of the overlapping of the different GDR components and of fluctuations of the orientation of the

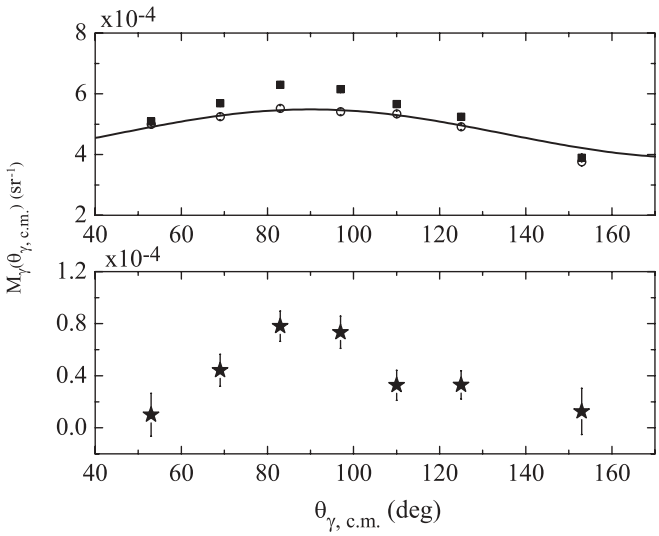

FIG. 10. (Top) Center-of mass angular distribution of the γ rays for the ^{36,40}Ar + ^{96,92}Zr reactions in the energy interval 10 MeV $\leqslant E_\gamma \leqslant$ 14 MeV corrected by the experimental setup efficiency. Solid squares, charge asymmetric (^{36}Ar + ^{96}Zr) reaction; open circles, charge symmetric (^{40}Ar + ^{92}Zr) reaction. The line is described in the text. (Bottom) Center-of mass angular distribution of the difference between the data of the two reactions in the same E_γ interval.

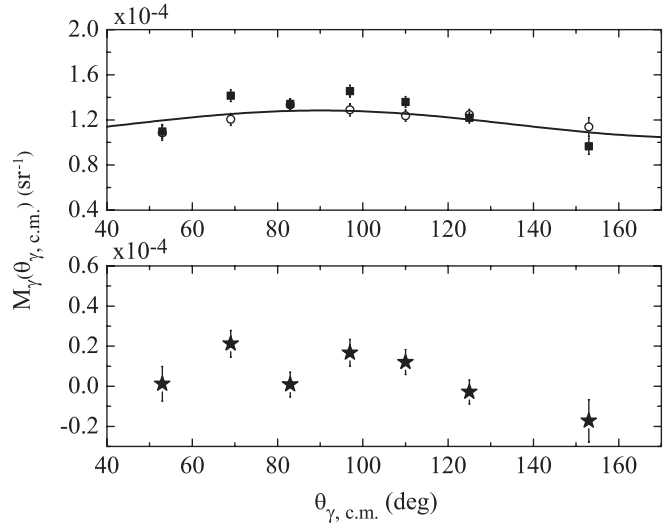

FIG. 11. The same as in Fig. 10 for the energy interval 15 MeV $\leqslant E_\gamma \leqslant$ 17 MeV.

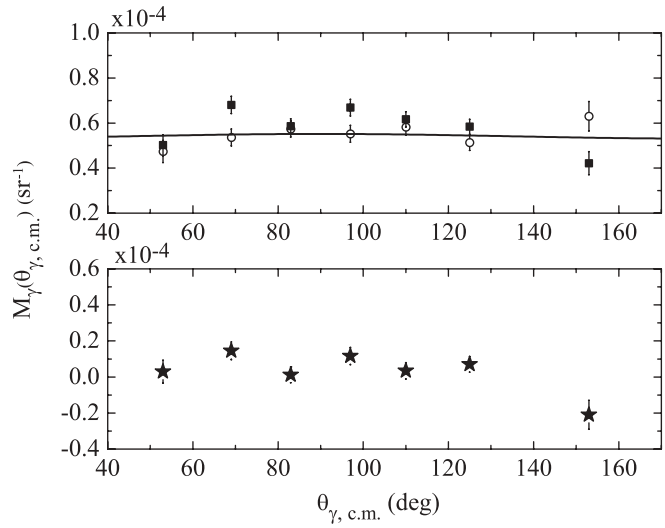

FIG. 12. The same as in Fig. 10 for the energy interval 18 MeV $\leqslant E_\gamma \leqslant$ 20 MeV.

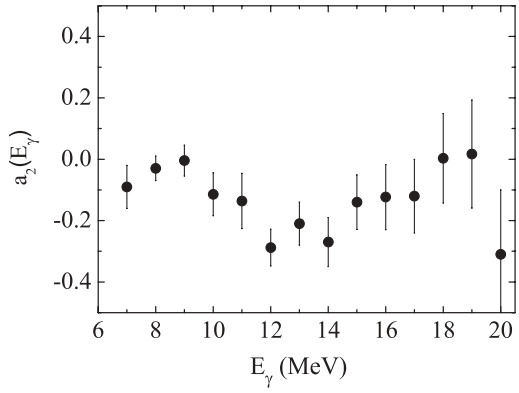

FIG. 13. Center-of-mass angular distribution coefficient $a_2(E_\gamma)$ for the symmetric reaction $^{40}\mathrm{Ar} + {}^{92}\mathrm{Zr}$.

angular frequency vector with respect to that of the density distribution [51]. Because, to our knowledge, there are no data on the GDR angular distribution at similar incident energies and in the Ce mass region, we compare this result with that of a previous measurement on the anisotropy of the GDR radiation that has been performed for the ^{109,110}Sn nucleus through the $^{48}\mathrm{Ti} + {}^{61,62}\mathrm{Ni}$ reactions at $E_{\mathrm{lab}} = 4.2$ and 4.6 MeV/nucleon, at $T \sim 1.8$ MeV, and for different spin intervals [52]. This comparison is appropriate, because the Sn nucleus is spherical in its ground state like the Ce one and it is expected to behave similarly with increasing spin and temperature. From the Sn data we see that for the low-energy GDR component the minimum a_2 is approximately -0.20 at a mean spin of $I = 49\hbar$ and at a mean temperature of $T = 1.4$ MeV. In the hypothesis of a mean spin of $I = 47$–$50\hbar$ in the $^{40}\mathrm{Ar} + {}^{92}\mathrm{Zr}$ reaction, our results on the a_2 coefficient (see Fig. 13) are compatible within errors with those of Ref. [52] at $I = 49\hbar$, though slightly higher in absolute value. A possible explanation can be found in the higher temperature achieved in the present experiment with respect to Ref. [52] which might lead to a larger most probable nuclear deformation and, thus, to a smaller attenuation of the a_2 coefficient absolute value.

In Fig. 14 we show the center-of-mass angular distribution of the difference between the data of the two reactions in the

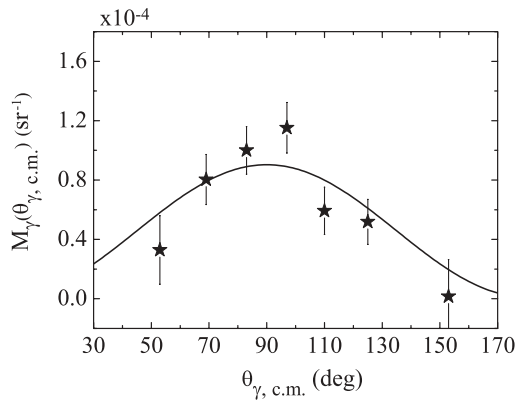

FIG. 14. Center-of mass angular distribution of the difference between the γ rays of the $^{36,40}\mathrm{Ar} + {}^{96,92}\mathrm{Zr}$ reactions in the energy interval 9 MeV $\leqslant E_\gamma \leqslant$ 21 MeV corrected by the experimental setup efficiency. The line in the figure is described in the text.

energy region from 9 to 21 MeV. We see that the experimental angular distribution is strongly anisotropic with a maximum around 90°. The data can be reasonably fitted with an $a_2 = -1$ coefficient, which results in an angular distribution of the $\sin^2(\theta_\gamma)$ form of emission from a dipole oscillation along the beam axis (solid line).

The direct dipole oscillation is expected to occur along the dinuclear system symmetry axis, which for near-central collisions forms a relatively small angle with the beam axis at the very early moments of its formation, as is shown in the following. We remind the reader that in the present experiment we consider the evaporation residues included in the contour of Fig. 2. Their average velocity is about 90% of the center-of-mass velocity, which indicates that we are dealing with near-central collisions [50,53]. The terms "central" and "near-central" collisions should be considered equivalent to the term "fusionlike" collisions, referring to large momentum transfer events (>85%) occurring at low-impact parameters where a large part of the projectile is captured by the target. Considering that the maximum angular momentum that the Ce nucleus can sustain without fissioning is $71\hbar$ (see the Introduction) and that the average transferred momentum is about 90%, we deduce a maximum impact parameter leading to fusionlike evaporation residues $b_{\mathrm{max}} = 3.5$ fm and a mean impact parameter $b_{\mathrm{mean}} = 2.3$–2.5 fm for a mean angular momentum of 47–$50\hbar$. For such a mean impact parameter the mean angle between the direct dipole axis and that of the beam at the early moments of the dinuclear system formation is about 14° for an interaction radius of $R = 9.5$ fm (calculated with $r_0 = 1.2$ fm). In the case of a larger mean inclination of the axis of the direct dipole oscillation, because rotation has taken place meanwhile, we would expect a widening of the angular distribution with respect to 90° and an anisotropy coefficient of $a_2 > -1$. This effect should be directly related to (a) the rotation angular velocity of the dinuclear system during the prompt dipole emission and (b) the instant at which this emission occurs.

The strong anisotropy of the γ-ray excess reported in Fig. 14 excludes the hypothesis of some remnant statistical GDR or np bremsstrahlung (direct or thermal) radiation in the difference spectrum and supports its origin in the dynamical dipole oscillation along an axis that has not rotated much with respect to the beam direction. Furthermore, it confines the γ-emission time scale at the very beginning of the reaction.

In perspective, we can say that accurate measurements of the dynamical dipole angular distribution could even allow one to directly evaluate the corresponding mean rotation of the emitting dinuclear system and then the time scale of such pre-equilibrium γ radiation.

IV. DISCUSSION

Calculations of the prompt dipole radiation for the Ar + Zr and S + Mo systems at different beam energies have been performed within the BNV transport model [9,10,54–58]. Within this model, in a microscopic approach based on semiclassical transport equations, where mean-field and two-body collisions are treated in a self-consistent way (for

details, see Ref. [9]), it has been studied how a collective dipole oscillation develops in the entrance channel. The numerical accuracy of the transport code has been largely improved to have reliable results also at low energies, just above the threshold for fusion reactions [9,10,54,55]. The mean-field dynamics within our semiclassical approach is very similar to the one obtained using time-dependent Hartree-Fock calculations [11]. However, our simulations include the effects of nucleon-nucleon collisions, which appear to be an essential ingredient for a realistic description of the reaction dynamics and the dynamical dipole at these energies. In the transport calculations no free parameters are used and an interesting dependence on the symmetry energy at low densities is observed. It is worth noting that within this framework a good description of the charge equilibration in peripheral heavy-ion collisions is achieved, confirmed by the observation of an extra dipole yield that depends on the centrality of the collision (see Ref. [15]).

In our theoretical analysis a dissipative reaction is described as developing through three main phases. The first is an *approaching phase* when the two partners overcome the Coulomb barrier still keeping their own response. The second is a *dinuclear phase* when the conversion of relative motion energy in thermal motion starts to take place, mainly due to nucleon exchange. The composite system is not thermally equilibrated and manifests, as a whole, a large amplitude dipole collective motion. The third phase consists of a thermally equilibrated nucleus decaying with consequent statistical particle/radiation emissions.

The second (*dinuclear*) phase can be characterized by pre-equilibrium collective dipole radiation emission with a contribution that can be estimated by applying a direct bremsstrahlung approach [12,58,59]. The total photon emission probability from the dipole mode oscillations can be expressed by the bremsstrahlung formula as ($E_\gamma = \hbar\omega$)

$$\frac{dP}{dE_\gamma} = \frac{2e^2}{3\pi\hbar c^3 E_\gamma}\left(\frac{NZ}{A}\right)^2 |X''(\omega)|^2, \qquad (6)$$

where $X''(\omega)$ is the Fourier transform of the acceleration $X''(t)$ associated with the distance between the centers of mass of protons (R_p) and neutrons (R_n), $X = R_p - R_n$, and $A = N + Z$ is the composite system mass. Thus following the time evolution of the dipole mode along the fusion dynamics it is possible to evaluate, in absolute values, the corresponding pre-equilibrium photon emission [12,58,59].

The employed mean-field transport approach describes properly the self-consistent couplings between various degrees of freedom. The potential part of the symmetry energy, $E_{\rm sym}/A$(pot),

$$\frac{E_{\rm sym}}{A} = \frac{E_{\rm sym}}{A}({\rm kin}) + \frac{E_{\rm sym}}{A}({\rm pot}) \equiv \frac{\epsilon_{\rm F}}{3} + \frac{{\rm C}(\rho)}{2\rho_0}\rho, \qquad (7)$$

is tested by employing two different density parametrizations, isovector equations of state (Iso-EoS) of the mean field: (i) $\frac{C(\rho)}{\rho_0} = 482 - 1638\rho$, (MeV fm^3), for "Asysoft" EoS, where $E_{\rm sym}/A$(pot) has a weak density dependence close to the saturation, with an almost flat behavior below ρ_0; and (ii) a constant coefficient, $C = 32$ MeV, for the "Asystiff" EoS choice, where the interaction part of the symmetry term displays a linear density dependence. As shown in details in Refs. [60] and [61] these choices represent two classes of widely used effective interactions that still require some confirmation from new independent observables. The isoscalar section of the EoS is the same in both cases, corresponding to a compressibility around 220 MeV. In the numerical simulations a test particle approach with 200 gaussian test particles per nucleon has been employed. In this way we get a good description of the phase space occupation, essential for the low-energy reaction dynamics. In the collision integral density dependent in-medium nucleon-nucleon (nn) cross sections are considered [62]. Different prescriptions are used to probe the sensitivity of the prompt radiation yield. We perform calculations for three impact parameters, $b = 0$, 2, and 4 fm, to cover the region where fusion is mostly observed. To reduce the numerical noise we run 20 events for each set of macroscopic initial conditions and the displayed quantities are the averages over this ensemble.

In our simulations the dynamical dipole yield for the more charge symmetric reactions, ^{40}Ar + ^{92}Zr and ^{36}S + ^{96}Mo, was found to be negligible. Therefore, the calculations presented in the following refer to the dynamical dipole yield related to the more charge asymmetric partner of each system, namely ^{36}Ar + ^{96}Zr and ^{32}S + ^{100}Mo. In Fig. 15 we present the total prompt dipole radiation yields evaluated (absolute values) for the ^{36}Ar + ^{96}Zr and ^{32}S + ^{100}Mo reactions, together with the available data (points in the figure) obtained by integrating the γ-ray excess over energy and over solid angle and by taking into account the corresponding experimental setup efficiency. In the integration of the data over solid angle an $a_2 = -1$ anisotropy coefficient for the dynamical dipole yield was considered. There are different sets of calculations. In the left-hand side of the figure we show theoretical calculations obtained with cross sections with an overall reduction (see Ref. [62]) corresponding to a constant nuclear density, $\rho = 0.14$ fm^{-3}, that is slightly lower than the saturation value $\rho = 0.17$ fm^{-3} for infinite nuclear matter (upper curves). In the same panel we show the results obtained using free nn cross sections (lower curves).

Reduced nn cross sections are leading to larger dipole radiation rates for two reasons: (i) less fast nucleon emission, in particular for neutrons that directly decrease the dipole strength, and (ii) reduced attenuation of the dipole pn oscillation due to a smaller number of pn direct collisions. In the right-hand side of the same figure we display the calculations done with in-medium reduced nn cross sections corresponding to nuclear densities that change "locally" during the reaction dynamics at each time step of the collisional procedure.

From Fig. 15 we can see the following. (1) The theoretical results for the above reactions (^{32}S + ^{100}Mo and ^{36}Ar + ^{96}Zr) are rather close, independent of the used nn cross section. According to Eq. (6), the total direct photon emission probability is systematically higher for the ^{36}Ar + ^{96}Zr reaction. However, differences are small, within 20%, and the direct comparison at different beam energies made in the present work is fully justified. (2) The experimental results for 6 and 16 MeV/nucleon are in good agreement with the theoretical ones if

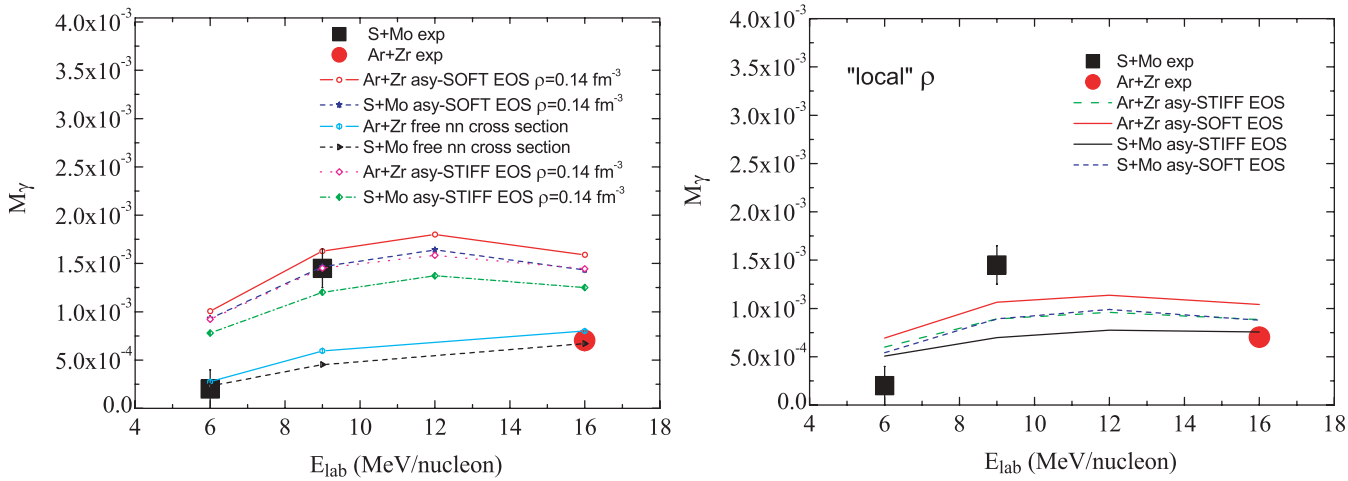

FIG. 15. (Color) (Left) Experimental multiplicity of the observed γ-ray excess integrated over energy and over solid angle corrected by the experimental setup efficiency and theoretical calculations obtained for free *nn* cross sections (lower curves) and for $\rho = 0.14$ fm^{-3} and in-medium reduced *nn* cross sections (upper curves). (Right) Experimental multiplicity as in the left-hand side of the figure and theoretical calculations for a local density as described in the text and in-medium reduced *nn* cross sections.

we use free *nn* cross sections but also if we use a "local" nuclear density and in-medium reduced *nn* cross sections. The experimental result obtained at 9 MeV/nucleon can be better reproduced by using reduced *nn* cross sections corresponding at constant nuclear density $\rho = 0.14$ fm^{-3}. In fact the calculation with "local nuclear density" modified cross sections gives a multiplicity approximately 40% (see right-hand side of the figure) lower than the experimental value at 9 MeV/nucleon. In any case the data show a maximum at 9 MeV/nucleon while the calculations have a smoother behavior with energy. Further investigation, from both a theoretical and an experimental point of view, around the maximum value of the dynamical dipole yield could give a more detailed mapping of its dependence on incident energy.

At higher beam energies the prompt dipole mode is expected to be overdamped because of a larger number of *np* collisions and fast neutron emissions. The isospin equilibration will then be ruled by a diffusion mechanism, again driven by the symmetry energy, as recently shown in Ref. [56].

From Fig. 15 we also see effects due to the density dependence of the symmetry term of the used interaction in the region below saturation, which is acting as a restoring force for the collective dipole oscillation of the dilute dinuclear system. Below ρ_0 the symmetry energy is larger for the Asysoft choice [60,61], and in correspondence we have some larger yields for the extra dipole radiation. However, we notice from Fig. 15 that we are not able to draw a conclusion about the density dependence of the symmetry energy by using stable beams. The reason is that the experimental errors, together with the small difference in the dynamical dipole yield according to the different theoretical prescriptions, do not allow one to discriminate among them. Radioactive beams are needed [58] to maximize the difference of the dynamical dipole yield between the different prescriptions of the symmetry energy dependence on density and allow an experimental discrimination.

The theoretical dynamical dipole centroid energies and widths were found to be $E_{\mathrm{dd,th}} \sim 9$ MeV and $\Gamma_{\mathrm{dd,th}} \sim 2$ MeV for all incident energies, thus in reasonable agreement with the corresponding experimental values (see Table I).

The transport simulations allow also a consistent calculation of the radiation anisotropies, i.e., of the coupling between the rotation of the dinuclear system and the γ emission (see details in Ref. [58]). The time scale of the radiative emission plays an essential role. Moreover, the calculations indicate that the largest contribution to the prompt γ yield is given by the first collective oscillations in a time interval of 200 fm/c (see Fig. 4 in Ref. [21]). Meanwhile the rotation of the symmetry axis is rather small (see Fig. 6 in Ref. [21]), and this is in agreement with our experimental finding of an almost pure dipole angular distribution with respect to the beam axis in near-central collisions. The symmetry energy in general is also slightly affecting the damping mechanisms and consequently the dinuclear rotation dynamics. We can expect to see a sensitivity to the slope of the symmetry term below saturation in the presence of large rotation, i.e., in events with high spin selection (see Ref. [58]).

V. CONCLUSIONS

In the present work the study of the evolution of the prompt dipole γ-ray emission with beam energy, started in Refs. [20] and [21], was pursued by investigating the fusion reactions ^{36}Ar + ^{96}Zr and ^{40}Ar + ^{92}Zr at $E_{\mathrm{lab}} = 16$ and 15.1 MeV/nucleon, respectively. These reactions lead to the same compound nucleus formed under identical conditions of spin and excitation energy as deduced from the analysis of the charged particle energy spectra in coincidence with fusionlike residues.

The 90° bremsstrahlung-subtracted γ-ray spectrum of the charge symmetric reaction ^{40}Ar + ^{92}Zr was analyzed in

the framework of the statistical model and a disappearance of the GDR above $E^* \sim 250$ MeV was deduced from the comparison with calculation, in good agreement with previous works for nuclei having similar mass. Then, a limiting excitation energy for the existence of collective motion in nuclei was shown also in the present work. Furthermore, the center-of-mass angular distribution of the charge symmetric reaction γ rays was found to be consistent with that of GDR γ decay from a hot rotating nucleus.

By studying the linearized 90° γ-ray spectra of the two reactions, a 12% increase of the γ-ray intensity was evidenced in the GDR energy region for the more charge asymmetric system, $^{36}\mathrm{Ar} + {}^{96}\mathrm{Zr}$, related to entrance channel effects. This result can be directly compared with those obtained for the reaction pair $^{32,36}\mathrm{S} + {}^{100,96}\mathrm{Mo}$ at lower incident energies, namely, at $E_{\mathrm{lab}} = 6$ MeV/nucleon [21] and 9 MeV/nucleon [20]. The prompt dipole γ-ray emission presents a maximum at incident energy of 9 MeV/nucleon decreasing toward lower and higher beam energies. The centroid energy and the width of the associated dynamical dipole mode were found to be constant, within errors, with beam energy.

The center-of-mass angular distribution of the observed extra γ yield in the charge asymmetric reaction is compatible with that of a dipole oscillating along the beam axis. That supports the pre-equilibrium character of the associated radiation because it suggests that it is emitted during the first moments of the dinuclear system formation, before any rotation has occurred.

The present experimental findings on the prompt dipole radiation are compared with theoretical calculations performed within the BNV transport model framework and based on a collective bremsstrahlung approach. The theoretical width and centroid energy of the dynamical dipole mode at all incident energies are in good agreement with the experimental values while the experimental angular distribution is in agreement with the theoretical expectations. However, the theoretical dynamical dipole yield, integrated over energy and over solid angle, is characterized by a behavior with incident energy smoother than that of the data that show a pronounced maximum at $E_{\mathrm{lab}} \sim 9$ MeV/nucleon and decrease toward lower and higher energies.

The dynamical dipole mode could represent a new cooling mechanism of the composite system, becoming thus of interest for the synthesis of super heavy elements. In fact, we know that the composite system survival probability against fission and the shell structure stabilization effects increase by decreasing the composite system excitation energy. The emission of pre-equilibrium dipole photons in charge asymmetric "hot" fusion reactions would produce a lowering of the compound nucleus excitation energy by about 10–15 MeV that could result in an increase of its survival probability against fission.

Furthermore, by using the prompt dipole radiation as a probe and employing radioactive beams, new possibilities for the investigation of the symmetry energy at subsaturation density are foreseen [57,58].

ACKNOWLEDGMENTS

We want to warmly acknowledge Massimo Loriggiola and Alberto Stefanini from the Legnaro National Laboratories (Italy) for providing us with the Zr targets and the LNS staff for the excellent quality of the beams. This work was supported in part by the Romanian Ministry for Education and Research under Contracts PNII, ID-946/2007, and ID-1038/2008.

[1] K. A. Snover, Annu. Rev. Nucl. Part. Sci. **36**, 545 (1986).
[2] J. J. Gaardhøje, Annu. Rev. Nucl. Part. Sci. **42**, 483 (1992).
[3] D. Santonocito and Y. Blumenfeld, Eur. Phys. J. A **30**, 183 (2006).
[4] M. Berlanger, A. Gobbi, F. Hanappe, U. Lynen, C. Ngô, A. Olmi, H. Sann, H. Stelzer, H. Richel, and M. F. Rivet, Z. Phys. A **291**, 133 (1979).
[5] M. Di Toro, C. Gregoire *et al.*, Z. Phys. A **320**, 321 (1985).
[6] D. Brink, Nucl. Phys. **A519**, 3c (1990).
[7] Ph. Chomaz, M. Di Toro, and A. Smerzi, Nucl. Phys. **A563**, 509 (1993).
[8] P. F. Bortignon, M. Braguti, D. M. Brink, R. A. Broglia, C. Brusati, F. Camera, W. Cassing, M. Cavinato, N. Giovanardi, and F. Gulminelli, Nucl. Phys. **A583**, 101c (1995).
[9] V. Baran, M. Colonna, M. Di Toro, A. Guarnera, and A. Smerzi, Nucl. Phys. **A600**, 111 (1996).
[10] V. Baran, M. Cabibbo, M. Colonna, M. Di Toro, and N. Tsoneva, Nucl. Phys. **A679**, 373 (2001).
[11] C. Simenel, Ph. Chomaz, and G. de France, Phys. Rev. Lett. **86**, 2971 (2001).
[12] V. Baran, D. M. Brink, M. Colonna, and M. Di Toro, Phys. Rev. Lett. **87**, 182501 (2001).
[13] C. H. Dasso, H. Sofia, and A. Vitturi, Eur. Phys. J. A **12**, 279 (2001).
[14] C. Simenel, Ph. Chomaz, and G. de France, Phys. Rev. C **76**, 024609 (2007).
[15] D. Pierroutsakou, M. Di Toro, F. Amorini, V. Baran, A. Boiano, A. De Rosa, A. D'Onofrio, G. Inglima, M. La Commara, A. Ordine, N. Pellegriti, F. Rizzo, V. Roca, M. Romoli, M. Sandoli, M. Trotta, and S. Tudisco, Eur. Phys. J. A **16**, 423 (2003); D. Pierroutsakou, A. Boiano, A. De Rosa, M. Di Pietro, G. Inglima, M. La Commara, A. Ordine, V. Roca, M. Romoli, M. Sandoli, M. Trotta, F. Rizzo, and L. Stroe, Nucl. Phys. **A687**, 245c (2001).
[16] F. Amorini, G. Cardella, A. Di Pietro, P. Figuera, G. Lanzalone, Lu Jun, A. Musumarra, M. Papa, S. Pirrone, F. Rizzo, W. Tian, and S. Tudisco, Phys. Rev. C **69**, 014608 (2004).
[17] M. Papa, W. Tian, G. Giuliani, F. Amorini, G. Cardella, A. Di Commara, P. P. Figuera, G. Lanzalone, S. Pirrone, F. Rizzo, and D. Santonocito, Phys. Rev. C **72**, 064608 (2005).
[18] S. Flibotte, Ph. Chomaz, M. Colonna, M. Cromaz, J. DeGraaf, T. E. Drake, A. Galindo-Uribarri, V. P. Janzen, J. Jonkman, S. W. Marshall, S. M. Mullins, J. M. Nieminen, D. C. Radford, J. L. Rodriguez, J. C. Waddington, D. Ward, and J. N. Wilson, Phys. Rev. Lett. **77**, 1448 (1996).
[19] M. Cinausero *et al.*, Nuovo Cimento **111**, 613 (1998).
[20] D. Pierroutsakou, A. Boiano, A. De Rosa, M. Di Pietro, G. Inglima, M. La Commara, R. Ming, B. Martin, R. Mordente, A. Ordine, F. Rizzo, V. Roca, M. Romoli, M. Sandoli, F. Soramel, L. Stroe, M. Trotta, and E. Vardaci, Eur. Phys. J. A **17**, 71 (2003).

[21] D. Pierroutsakou, B. Martin, G. Inglima, A. Boiano, A. De Rosa, M. Di Commara, M. La Commara, R. Mordente, M. Romoli, M. Sandoli, M. Trotta, E. Vardaci, T. Glodariu, M. Mazzocco, C. Signorini, L. Stroe, V. Baran, M. Colonna, M. Di Toro, and N. Pellegriti, Phys. Rev. C **71**, 054605 (2005).

[22] W. J. Swiatecki, Phys. Scr. **24**, 113 (1981).

[23] M. Thoennessen, E. Ramakrishnan, J. R. Beene, F. E. Bertrand, M. L. Halbert, D. J. Horen, P. E. Mueller, and R. L. Varner, Phys. Rev. C **51**, 3148 (1995).

[24] A. Gavron, Phys. Rev. C **21**, 230 (1980).

[25] B. Martin, D. Pierroutsakou, C. Agodi, R. Alba, V. Baran, A. Boiano, G. Cardella, M. Colonna, R. Coniglione, E. De Filippo, A. De Rosa, A. Del Zoppo, M. Di Toro, G. Inglima, T. Glodariu, M. La Commara, C. Maiolino, M. Mazzocco, A. Pagano, P. Piattelli, S. Pirrone, C. Rizzo, M. Romoli, M. Sandoli, D. Santonocito, P. Sapienza, and C. Signorini, Phys. Lett. **B664**, 47 (2008).

[26] D. Pierroutsakou, B. Martin, G. Inglima, A. Boiano, A. De Rosa, M. Di Pietro, M. La Commara, R. Mordente, M. Romoli, M. Sandoli, M. Trotta, E. Vardaci, T. Glodariu, M. Mazzocco, C. Signorini, L. Stroe, C. Agodi, R. Alba, M. Colonna, R. Coniglione, A. Del Zoppo, M. Di Toro, C. Maiolino, N. Pellegriti, P. Piattelli, D. Santonocito, P. Sapienza, G. Cardella, E. De Filippo, A. Pagano, S. Pirrone, and V. Baran, in *Proceedings of the 5th Italy-Japan Symposium: Recent Achievements and Perspectives in Nuclear Physics, Naples, Italy, 2004*, edited by G. La Rana *et al.* (World Scientific, Singapore, 2005), p. 121.

[27] D. Pierroutsakou, B. Martin, G. Inglima, C. Agodi, R. Alba, V. Baran, A. Boiano, G. Cardella, M. Colonna, R. Coniglione, E. De Filippo, A. De Rosa, A. Del Zoppo, M. Di Pietro, M. Di Toro, T. Glodariu, M. La Commara, C. Maiolino, M. Mazzocco, A. Pagano, N. Pellegriti, P. Piattelli, S. Pirrone, M. Romoli, M. Sandoli, D. Santonocito, P. Sapienza, and C. Signorini, AIP Conf. Proc. **884**, 201 (2006).

[28] B. Martin, D. Pierroutsakou, G. Inglima, A. Boiano, A. De Rosa, M. Di Pietro, M. La Commara, M. Romoli, M. Sandoli, C. Agodi, R. Alba, G. Cardella, M. Colonna, R. Coniglione, E. De Filippo, A. Del Zoppo, M. Di Toro, C. Maiolino, A. Pagano, N. Pellegriti, P. Piattelli, S. Pirrone, D. Santonocito, P. Sapienza, V. Baran, T. Glodariu, M. Mazzocco, and C. Signorini, AIP Conf. Proc. **831**, 505 (2005).

[29] B. Martin, D. Pierroutsakou, G. Inglima, A. Boiano, A. De Rosa, M. La Commara, M. Romoli, M. Sandoli, C. Agodi, R. Alba, R. Coniglione, A. Del Zoppo, C. Maiolino, P. Piattelli, D. Santonocito, P. Sapienza, G. Cardella, E. De Filippo, A. Pagano, S. Pirrone, T. Glodariu, M. Mazzocco, and C. Signorini, Acta Phys. Pol. B **38**, 1473 (2007).

[30] E. Migneco, C. Agodi, R. Alba, G. Bellia, R. Coniglione, A. Del Zoppo, P. Finocchiaro, C. Maiolino, P. Piattelli, G. Raia, and P. Sapienza, Nucl. Instrum. Methods Phys. Res. A **314**, 31 (1992).

[31] T. Matulewicz, E. Grosse, H. Emling, H. Grein, and R. Kulessa, Nucl. Instrum. Methods Phys. Res. A **274**, 501 (1989).

[32] S. Kubota, T. Motobayashi, M. Ogiwara, H. Murakami, Y. Ando, J. Ruan, and S. Shirato, Nucl. Instrum. Methods Phys. Res. A **285**, 436 (1989).

[33] A. Del Zoppo, C. Agodi, R. Alba, G. Bellia, R. Coniglione, P. Finocchiaro, C. Maiolino, E. Migneco, A. Peghaire, P. Piattelli, and P. Sapienza, Nucl. Instrum. Methods Phys. Res. A **327**, 363 (1993).

[34] H. Morgenstern, W. Bohne, W. Galster, K. Grabisch, and A. Kyanowski, Phys. Rev. Lett. **52**, 1104 (1984).

[35] M. P. Kelly, J. F. Liang, A. A. Sonzogni, K. A. Snover, J. P. S. van Schagen, and J. P. Lestone, Phys. Rev. C **56**, 3201 (1997).

[36] E. Holub, D. Hilscher, G. Ingold, U. Jahnke, H. Orf, and H. Rossner, Phys. Rev. C **28**, 252 (1983).

[37] M. P. Kelly, K. A. Snover, J. P. S. van Schagen, M. Kicinska-Habior, and Z. Trznadel, Phys. Rev. Lett. **82**, 3404 (1999).

[38] R. Ortega, D. d'Enterria, G. Martínez, D. Baiborodin, H. Delagrange, J. Díaz, J. Fernández, H. Löhner, T. Matulewicz, R. W. Ostendorf, S. Schadmand, Y. Schutz, P. Tlusty, R. Turrisi, V. Wagner, H. W. Wilschut, and N. Yahlali, Eur. Phys. J. A **28**, 161 (2006).

[39] H. Nifenecker and J. A. Pinston, Annu. Rev. Nucl. Part. Sci. **40**, 113 (1990).

[40] R. Alba, C. Maiolino, C. Agodi, A. Del Zoppo, R. Coniglione, P. M. Milazzo, P. Sapienza, G. Bellia, M. Bruno, M. Colonna, N. Colonna, M. D'Agostino, M. L. Fiandri, P. Finocchiaro, F. Gramegna, I. Iori, K. Loukachine, G. V. Margagliotti, P. F. Mastinu, E. Migneco, A. Moroni, P. Piattelli, R. Rui, D. Santonosito, F. Tonetto, and G. Vannini, Nucl. Phys. **A654**, 761c (1999).

[41] Y. Schutz, G. Martínez, F. M. Marqués, A. Marín, T. Matulewicz, R. W. Ostendorf, P. Bożek, H. Delagrange, J. Díaz, M. Franke, K. K. Gudima, S. Hlaváč, R. Holzmann, P. Lautridou, F. Lefèvre, H. Löhner, W. Mittig, M. Ploszajczak, J. H. G. van Pol, J. Québert, P. Roussel-Chomaz, A. Schubert, R. H. Siemssen, R. S. Simon, Z. Sujkowski, V. D. Toneev, V. Wagner, H. W. Wilschut, and Gy. Wolf, Nucl. Phys. **A622**, 404 (1997).

[42] F. Puhlhofer, Nucl. Phys. **A280**, 267 (1977); M. N. Harakeh, extended version (private communication).

[43] G. Bellia, R. Alba, R. Coniglione, A. Del Zoppo, P. Finocchiaro, C. Maiolino, E. Migneco, P. Piattelli, P. Sapienza, N. Frascaria, I. Lhenry, J. C. Roynette, T. Suomijärvi, N. Alamanos, F. Auger, A. Gillibert, D. Pierroutsakou, J. L. Sida, and P. R. Silveira Gomes, Nucl. Instrum. Methods Phys. Res. A **329**, 173 (1993).

[44] D. Pierroutsakou, F. Auger, N. Alamanos, P. R. S. Gomes, J. L. Sida, A. Gillibert, N. Frascaria, I. Lhenry, J. C. Roynette, and T. Suomijärvi, Nucl. Phys. **A600**, 131 (1996).

[45] T. Suomijärvi, Y. Blumenfeld, P. Piattelli, J. H. Le Faou, C. Agodi, N. Alamanos, R. Alba, F. Auger, G. Bellia, Ph. Chomaz, R. Coniglione, A. Del Zoppo, P. Finocchiaro, N. Frascaria, J. J. Gaardhøje, J. P. Garron, A. Gillibert, M. Lamehi-Rachti, R. Liguori-Neto, C. Maiolino, E. Migneco, G. Russo, J. C. Roynette, D. Santonocito, P. Sapienza, J. A. Scarpaci, and A. Smerzi, Phys. Rev. C **53**, 2258 (1996).

[46] J. J. Gaardhøje, A. M. Bruce, J. D. Garrett, B. Herskind, D. Barneoud, M. Maurel, H. Nifenecker, J. A. Pinston, P. Perrin, C. Ristori, F. Schussler, A. Bracco, and M. Pignanelli, Phys. Rev. Lett. **59**, 1409 (1987).

[47] D. Santonocito, P. Piattelli, Y. Blumenfeld, T. Suomijärvi, C. Agodi, N. Alamanos, R. Alba, F. Auger, G. Bellia, Ph. Chomaz, M. Colonna, R. Coniglione, A. Del Zoppo, P. Finocchiaro, N. Frascaria, A. Gillibert, J. H. Le Faou, K. Loukachine, C. Maiolino, E. Migneco, J. C. Roynette, P. Sapienza, and J. A. Scarpaci, Phys. Rev. C **66**, 044619 (2002).

[48] J. B. Natowitz, R. Wada, K. Hagel, T. Keutgen, M. Murray, A. Makeev, L. Qin, P. Smith, and C. Hamilton, Phys. Rev. C **65**, 034618 (2002).

[49] M. E. Rose, Phys. Rev. **91**, 610 (1953).
[50] P. Piattelli, D. Santonocito, Y. Blumenfeld, T. Suomijärvi, C. Agodi, N. Alamanos, R. Alba, F. Auger, G. Bellia, Ph. Chomaz, M. Colonna, R. Coniglione, A. Del Zoppo, P. Finocchiaro, N. Frascaria, A. Gillibert, J. H. Le Faou, K. Loukachine, C. Maiolino, E. Migneco, J. C. Roynette, P. Sapienza, and J. A. Scarpaci, Phys. Lett. **B442**, 48 (1998).
[51] Y. Alhassid and B. Bush, Phys. Rev. Lett. **65**, 2527 (1990).
[52] A. Bracco, F. Camera, M. Mattiuzzi, B. Million, M. Pignanelli, J. J. Gaardhøje, A. Maj, T. Ramsøy, T. Tveter, and Z. Źelazny, Phys. Rev. Lett. **74**, 3748 (1995).
[53] V. E. Viola, Jr., B. B. Back, K. L. Wolf, T. C. Awes, C. K. Gelbke, and H. Breuer, Phys. Rev. C **26**, 178 (1982).
[54] M. Cabibbo, V. Baran, M. Colonna, and M. Di Toro, Nucl. Phys. **A637**, 374 (1998).
[55] C. Rizzo, Ph.D. thesis, Università di Catania, 2007.
[56] J. Rizzo, M. Colonna, V. Baran, M. Di Toro, H. H. Wolter, and M. Zielinska-Pfabe, Nucl. Phys. **A806**, 79 (2008); V. Baran, M. Colonna, M. Di Toro, M. Zielinska-Pfabe, and H. H. Wolter, Phys. Rev. C **72**, 064620 (2005).
[57] M. Di Toro, M. Colonna, C. Rizzo, and V. Baran, Int. J. Mod. Phys. E **17**, 110 (2009).
[58] V. Baran, C. Rizzo, M. Colonna, M. Di Toro, and D. Pierroutsakou, Phys. Rev. C **79**, 021603(R) (2009).
[59] A bremsstrahlung approach [T. Papenbrock and G. F. Bertsch, Phys. Rev. Lett. **80**, 4141 (1998)] was applied to calculate the photon emission during the α-decay process. In our calculations the classical bremsstrhalung appears justified because the dynamics is well above the threshold and so in a classical allowed region.
[60] V. Baran, M. Colonna, V. Greco, and M. Di Toro, Phys. Rep. **410**, 335 (2005).
[61] Bao-An Li, Lie-Wen Chen, and Che Ming Ko, Phys. Rep. **464**, 113 (2008).
[62] G. Q. Li and R. Machleidt, Phys. Rev. C **49**, 566 (1994).